CrystEngComm

Accepted Manuscript

This article can be cited before page numbers have been issued, to do this please use: P. Das, S. Bhandary, D. Mathew, A. Dutta, K. P. Dhabhai, S. K. Seth and D. Chopra, *CrystEngComm*, 2026, DOI: 10.1039/D5CE00838G.




ROYAL SOCIETY OF CHEMISTRY

rsc.li/crystengcomm

View Article Online
DOI: 10.1039/D5CE00838G

# *Investigation of noncovalent interactions in organofluorine compounds with C-F bonds in different electronic environment*

*Prantika Das[†], Subhrajyoti Bhandary[§], Dona Mathew[§], Arnab Dutta[§], Kanu Priya Dhabhai[§], Saikat Kumar Seth[†*], and Deepak Chopra[§ *]*

*[†]Department of Physics, Jadavpur University, Kolkata 700032, India.*

*[§] Department of Chemistry, Indian Institute of Science Education and Research Bhopal, Bhopal, Madhya Pradesh 462066, India.*

*Email: saikatk.seth@jadavpuruniversity.in (SKS); dchopra@iiserb.ac.in (DC)*

***Dedicated to Professor Resnati, celebrating a career in fluorine and noncovalent chemistry on the occasion of his 70th birthday.***

**Abstract:** We have synthesized a series of fluorine substituted 2-methylpropanamide compounds including a pair of polymorphs with the fluorine substitution at aromatic ring and methyl carbon to investigate the relevance of weak non-covalent interactions in the solid-state. The compounds are structurally characterized by single crystal X-ray diffraction technique and their supramolecular behaviour are explored methodically regarding the contribution of strong hydrogen bonds like N–H···O, acting in conjunction with C–H···O, and the ancillary support of weak C–H···F interaction. PIXEL calculations allowed for the estimation of the different intermolecular interaction energies of the derived dimers and the overall lattice energies of the different crystalline solids. It is observed that the molecular motifs consisting of C($sp^2$)–H···F–C($sp^2$) interaction are more stable in comparison to other C–H···F interactions. QTAIM analysis further supports these interactions via a topological analysis of the electron density distribution at the bond critical point. A detailed experimental and computational evaluation have been carried out to evaluate the effect of the environment surrounding the carbon atom, i.e. the role of hybridization of the carbon atom, connected to the acceptor fluorine atom and the donor hydrogen atom as well.

## Introduction

The contribution of organic fluorine in the formation of weak interactions and the reinforcement of the molecular crystal has been an important topic of discussion over the past

View Article Online
DOI: 10.1039/D5CE00838G



few years.[1] There is a substantial body of literature in which the significance of intermolecular interactions involving organic fluorine and their exclusive involvement in controlling the crystal structures are well-explored through different computational and experimental approaches.[2–4] The role of strong and conventional hydrogen bonds in controlling the crystal architects has been reliable[5] but the independent existence of these weak interactions involving organic fluorine, instead of strong hydrogen bonds, is still under consideration.[6–8] From previous studies, among all these weak interactions, the important contribution of C–H···F interaction in the stabilization has been recognized despite the presence of strong hydrogen bonds.[9] However, the hybridization of the carbon atom attached to the fluorine and the hydrogen atoms has a subtle impact on the stability of the bond, the participation of fluorine atom in the formation of different stable motifs and the robustness of those motifs in the systematic exploration of supramolecular assemblies.[10, 11] In this context, C–H···F interaction can be classified into four categories: C($sp^3$)–H···F–C($sp^3$), C($sp^3$)–H···F–C($sp^2$), C($sp^2$)–H···F–C($sp^3$), and C($sp^2$)–H···F–C($sp^2$). Greater is the s-character of carbon atom attached to hydrogen; more is the acidic nature of the participating hydrogen atom and thus resulting in higher stability of the hydrogen bondformed.[12–13]

Majority investigations in the past involved the presence of a fluorine atom connected to aromatic ring carbon atom ($sp^2$ hybridized).[11, 14–15] Lately, the capability of a fluorine atom attached to a $sp^3$ hybridized carbon atom has been investigated in the generation of different structural motifs and their effect on crystal packing in a series of isomeric trifluoromethyl-substituted benzanilides.[16] The charge density analysis reveals the intrinsic polarization of the electron density on the fluorine atom in the trifluoromethyl group.[17] Another study including a series of substituted benzanilides consisting of both fluorine and trifluoromethyl group unveils that C($sp^2$)–H···F–C($sp^2$) hydrogen bonds preferably inculcate the highest stabilized molecular motifs in comparison to C($sp^2$)–H···F–C($sp^3$) interactions.[18] Furthermore, in a recent study the electronic environment of the donor hydrogen and acceptor fluorine atoms has been varied in a series of fluorine substituted propanamide compounds and consequently their influence in the molecular motifs and crystal packing have been comprehensively studied by analysing X-ray data.[19] However, the study indicates that the interaction energy is relatively higher for C($sp^2$)–H···F–C($sp^2$) interactions and variations in the interaction energies ie the local stabilization energies, and the charge densities is noticed while considering C($sp^3$)–H···F–C($sp^3$), C($sp^3$)–H···F–C($sp^2$), C($sp^2$)–H···F–C($sp^3$) interactions.

View Article Online
DOI: 10.1039/D5CE00838G



Contemplating with the results of previous studies, a comprehensive study has been aimed to analyse the supporting role of weak C–H···F interactions in regulating crystalline solids, considering different electronic environment around the donor hydrogen and the acceptor fluorine atom. For this purpose, a series of propanamide compounds have been synthesized where fluorine is substituted at the *ortho*, *meta*, and *para* positions of the aromatic ring ($sp^2$ hybridization), and at a methyl carbon ($sp^3$ hybridization). The current study has four objectives. Firstly, the compounds are synthesized, crystallized and the molecular structures are determined by single crystal X-ray diffraction. Secondly, the salient features of the crystal packing incorporating strong along with weak intermolecular interactions have been explored thoroughly. Next, PIXELC method has been utilized to derive the molecular motifs consisting of weak C–H···F interactions in the presence of strong hydrogen bonds and their interaction energies are evaluated. Furthermore, analysis of the topological parameters at the bond critical points has been performed to showcase the nature of these interactions. Moreover, an attempt is made to perceive the trend that unveils the influence of the hybridization of carbon in the formation of favourable C–H···F interactions.

**Experimental Section:**

**Synthesis and Crystallization of the compounds 1, 2, and 3:** The fluoro-substituted organic acid (1.50 mmol, 0.14 mL) (**Scheme 1**) was placed in a 25 mL round-bottom flask and dissolved in 4 mL dichloromethane (DCM). Two drops of DMF were added under $N_2$ atmosphere and the flask was cooled in an ice bath. Oxalyl chloride (1.80 mmol, 0.15 mL) was then added dropwise at the same temperature (0 ºC). The resulting reaction mixture was stirred at room temperature for 8 h. After complete consumption of the starting material, as monitored by thin layer chromatography (TLC), the solvent and excess oxalyl chloride was removed under reduced pressure in an inert atmosphere. The yellow-coloured liquid (the corresponding acid chloride) was obtained which was used in the next step without further purification.

Subsequently, the obtained acid chloride (1.50 mmol, 0.14 mL), was dissolved in 4 mL of DCM under $N_2$ atmosphere at 0 ºC. Triethylamine (9.00 mmol, 1.2 mL) and the corresponding fluoro-substituted aniline (1.50 mmol, 0.14 mL) were added to the solution at the same temperature. The reaction mixture was stirred at room temperature for 10 h. Upon completion of the reaction, as monitored by TLC, reaction mixture was quenched with water and 5% HCl and extracted with DCM (50 mL × 3). The organic layer was collected, dried over anhydrous sodium sulphate and the solvent was then evaporated under reduced pressure. The resulting crude compound was purified by column chromatography (with a solvent mixture of ethyl

View Article Online
DOI: 10.1039/D5CE00838G

acetate and hexane as the eluent) to obtain compounds **1, 2** and **3** as white solid in 54%, 50% and 51% yields, respectively.

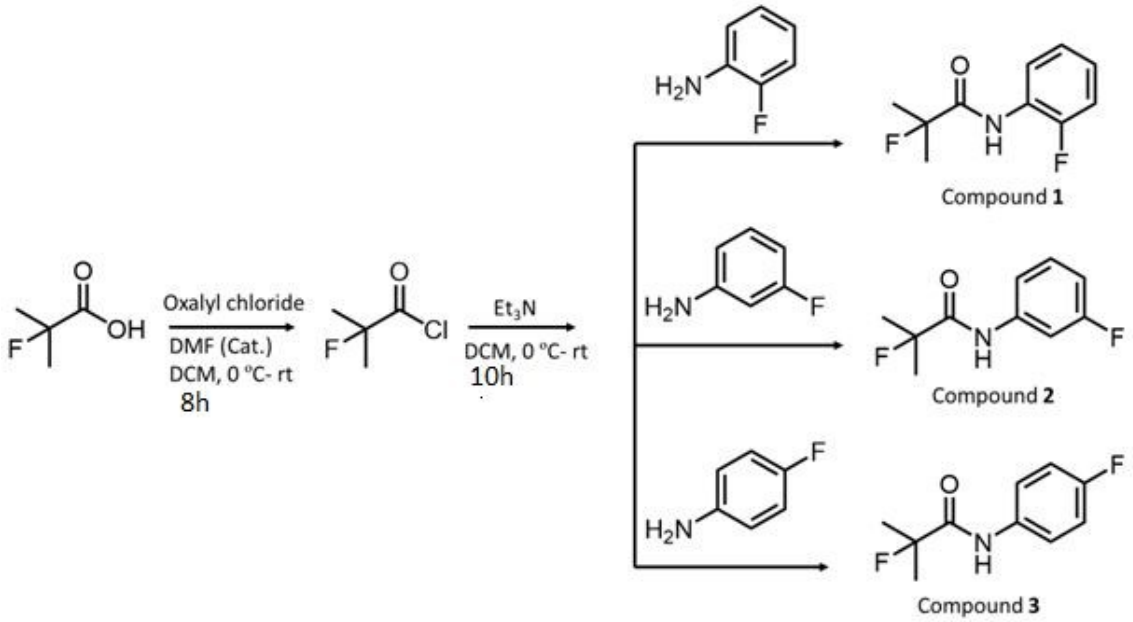


**Scheme 1:** Chemical Scheme depicting the synthetic procedure for the obtained compounds.

The compounds were dissolved in different organic solvents, namely, ethyl acetate/hexane, dichloromethane (DCM)/hexane, ethanol, toluene, $CDCl_3$, acetone and benzene. In most of the cases, aggregates were obtained. The crystals obtained via slow evaporation of solvents at both ambient (24-28°C) and low temperature (4°C) were examined under an optical microscope and further screened for collection of the X-ray diffraction data. The solvent system from which final crystals utilized for measurement of diffraction were obtained is mentioned in Table 1.

***Nuclear Magnetic Resonance (NMR) Spectroscopy***

$^1$H NMR spectra were conducted on a Bruker Avance Neo 500 MHz spectrometer for all compounds using $CDCl_3$ and DMSO-$d_6$ as solvents. The spectral analysis is provided in Figures S1-S3.

***Liquid Chromatography-Mass Spectrometry (LC-MS)***

The experiments were executed through a Bruker micrOTOF-Q II mass spectrometer. There was a good correlation observed between calculated mass and experimental mass for all the compounds (Figure S4).

***Molecular Structure Determination by Single Crystal X-ray Diffraction***

View Article Online
DOI: 10.1039/D5CE00838G



All compounds are structurally characterized by single crystal X-ray diffraction using Bruker APEX–II CCD single crystal diffractometer equipped with a graphite monochromator, $MoK_\alpha$ radiation (λ=0.71073 Å) controlled by APEX2.[20]The data collection were performed at105(2) K, 103(2) K, 102(2) K and 94(2) K for (**1**), (**2**), **3-Form–I** and **3-Form–II** respectively. Data were corrected for Lorentz and polarization effects using SAINT.[21] The absorption correction was done using the multi-scan method using SADABS-2014/2.[22] The structures are solved by direct methods using SHELXT 2014/5[23] and refined by full-matrix least-squares method using the SHELXL-2016/6 program.[24] All non-hydrogen atoms are refined anisotropically, and all hydrogen atoms bound to carbon atoms are placed in the calculated positions where thermal parameters are refined isotropically with $U_{eq}$= 1.2–1.5$U_{eq}$(C). The hydrogen atoms attached to nitrogen atoms are located from the difference Fourier map and refined isotropically with $U_{eq}$= 1.2$U_{eq}$(N). All structural geometrical parameters are derived using PLATON.[25] The geometrical parameters related to hydrogen bonds are analysed form the.lst file from PARST program.[26] The 4-fluorophenyl ring in **3_Form_II** is disordered in the 1:1 ratio. Only one conformer has been considered for further discussions. Details of the X-ray measurements and crystal parameters of all the compounds are given in Table 1. The weak intermolecular interactions are considered based on the following criteria: the sum of the vdW's radii + 0.2Å and directionality ≥110° and are further validated via QTAIM calculations.

***Theoretical Calculations***

The lattice energies for all four compounds are calculated using PIXELC method in CLP module.[27]The interaction energies estimated for molecular pairs are partitioned in four types of energy terms: Coulombic ($E_{coul}$), polarization ($E_{pol}$), dispersion ($E_{disp}$), and repulsion ($E_{rep}$).[28, 29] For this purpose, the wave function related to electron density of the molecules are obtained by DFT theory at the B3LYP/6311++G(d,p) basis set using Gaussian16[30] considering H atoms at their neutron distances. The percentage contribution of electrostatic and dispersion energy towards total stabilization is calculated as:

$$\%E_{disp} = \left[\frac{E_{disp}}{E_{Coul} + E_{pol} + E_{disp}}\right] \times 100 \quad (1)$$

$$\%E_{elec} = 100 - \%E_{disp} \quad (2)$$

Molecular Hirshfeld surfaces[31, 32]generated through CrystalExplorer21.5[33] are mapped over normalised contact distance ($d_{norm}$), shape index and curvedness surfaces. The existence of red, white and blue dots on $d_{norm}$ surface indicate the shorter contacts, contacts around vdW separation and longer contacts respectively. The percentage contribution of each possible

View Article Online
DOI: 10.1039/D5CE00838G

contacts has been represented by decomposed 2D fingerprint plots[34–37] composed by $d_e$ (the distance from the point to the nearest nucleus external to the surface) and $d_i$ distances (the distance from the point nearest nucleus internal to the surface). Moreover, the lattice energy[38] of all compounds has been computed using *CrystalExplorer21.5* through an accurate method B3LYP/6–31G(d,p) given in section S.1. (Table S3).

Consequently, the molecular pairs comprising of C–H···F interactions are taken into consideration to characterize the interactions the "quantum theory of atoms in molecules" (QTAIM)[39]using AIMALL software.[40]This analysis includes the topological parameters such as electron charge density ($\rho(r)$), Laplacian of electron charge density ($\nabla^2(\rho(r)$, local potential energy density (($V(r)$), kinetic energy density (($G(r)$), and total energy density (($H(r)$). The interaction energy($E_{int}$)is calculated by the method proposed by Epinosa[41] using the local potential energy density (($V(r)$) as $E_{int} = -313.754 \times V(r)$ (in kcal/mol).[42]

**Table 1:** Crystal and refinement data of compounds (**1**–**2**), **3-Form-I** and **3-Form-II**.

| Sample code | (1) | (2) | 3-Form-I | 3-Form-II |
|---|---|---|---|---|
| **Formula** | $C_{10}H_{11}F_2NO$ | $C_{10}H_{11}F_2NO$ | $2(C_{10}H_{11}F_2NO)$ | $C_{10}H_{11}F_2NO$ |
| **Formula weight** | 199.20 | 199.20 | 398.39 | 199.20 |
| **Temperature (K)** | 105(2) | 103(2) | 102(2) | 94(2) |
| **Wavelength (Å)** | 0.71073 | 0.71073 | 0.71073 | 0.71073 |
| **Solvent** | DCM and hexane (3:1) | DCM | Toluene | DCM and hexane (3:1) |
| **CCDC number** | 2483272 | 2483273 | 2483274 | 2483275 |
| **Crystal system** | Orthorhombic | Orthorhombic | Monoclinic | Triclinic |
| **Space group** | $P2_12_12_1$ | $Pca2_1$ | $P2_1/n$ | $P\bar{1}$ |
| **a (Å)** | 5.1128(8) | 12.0624(7) | 9.5100(11) | 5.1799(14) |
| **b (Å)** | 6.7751(11) | 9.4612(6) | 11.0959(13) | 9.618(3) |
| **c (Å)** | 27.331(5) | 8.6588(4) | 19.198(2) | 10.442(3) |
| **α (°)** | 90 | 90 | 90 | 81.822(9) |
| **β (°)** | 90 | 90 | 102.991(4) | 80.772(9) |
| **γ (°)** | 90 | 90 | 90 | 74.442(9) |
| **V (Å³)** | 946.8(3) | 988.18(10) | 1974.0(4) | 491.9(2) |
| **Z** | 4 | 4 | 4 | 2 |
| **Density (g cm$^{-3}$)** | 1.398 | 1.339 | 1.341 | 1.345 |
| **μ (mm$^{-1}$)** | 0.117 | 0.112 | 0.112 | 0.113 |
| **F(000)** | 416 | 416 | 832 | 208 |
| **θ (min, max)** | 3.098, 30.133 | 2.736, 30.036 | 2.177, 29.130 | 2.210, 30.357 |

| Treatment of hydrogen atoms | Mixed | Mixed | Constrained | Constrained |
|---|---|---|---|---|
| $h_{min, max}$, $k_{min, max}$, $l_{min, max}$ | (–7, 5), (–9, 9), (–38, 37) | (–16, 16), (–13, 13), (–9, 12) | (–13, 11), (–15, 15), (–26, 23) | (–7, 7), (–13, 13), (–14, 14) |
| No. of total ref. | 9776 | 8140 | 22866 | 16517 |
| No. of unique/obs ref. | 2790/2274 | 2362/ 2058 | 5283/3423 | 2947/1714 |
| No. of parameters | 133 | 133 | 257 | 165 |
| $R_{all}$, $R_{obs}$ | 0.0580, 0.0394 | 0.0519, 0.0408 | 0.0917, 0.0477 | 0.1221, 0.0548 |
| $wR_{2all}$, $wR_{2obs}$ | 0.0844, 0.0786 | 0.1039, 0.0989 | 0.1156, 0.0998 | 0.1400, 0.1181 |
| $\Delta\rho_{min, max}$ (eÅ$^{-3}$) | –0.194, 0.271 | –0.264, 0.413 | –0.246, 0.329 | –0.253, 0.285 |
| G. O. F. | 1.036 | 1.044 | 1.030 | 1.047 |

## Results and Discussion

### Analysis of molecular structure and crystal packing of compounds (1-2, 3-Form-I & II)

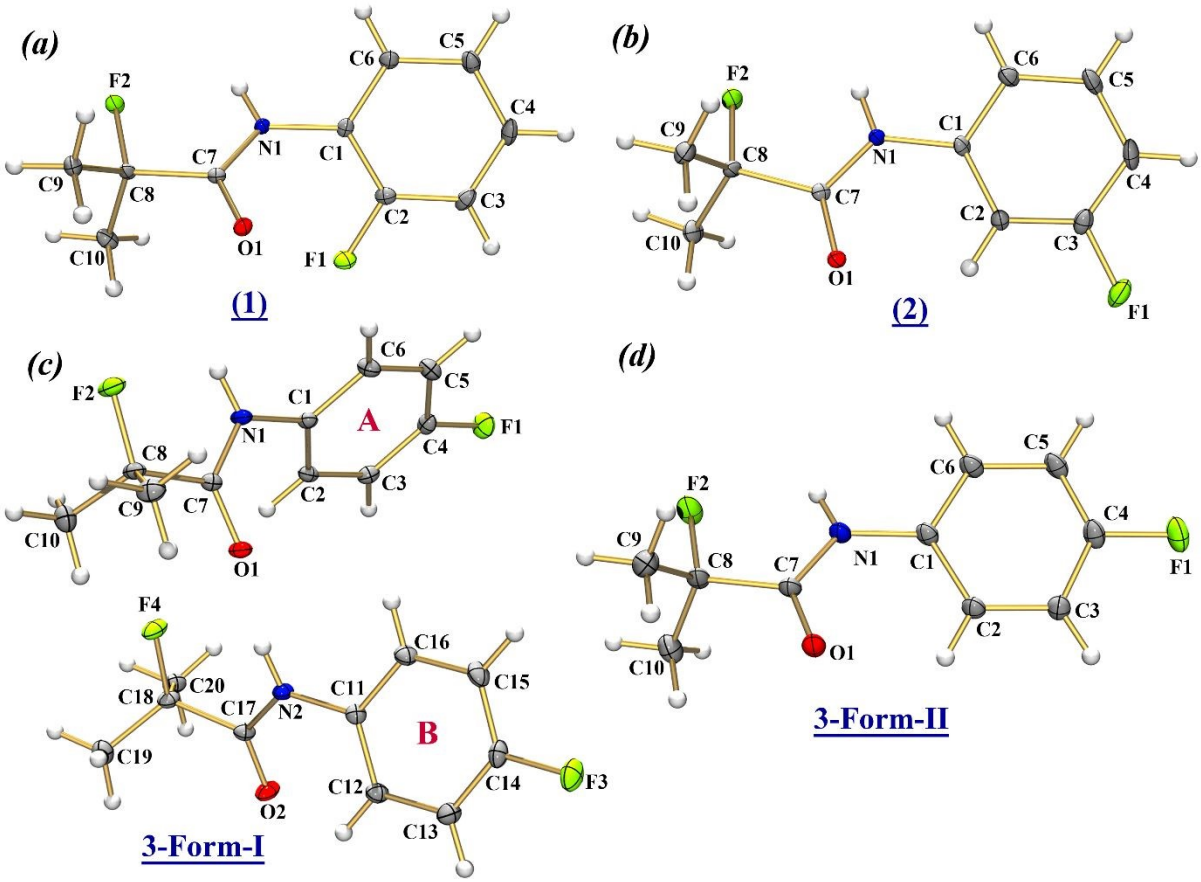


**Figure 1.***ORTEP* of compound (**a**)(**1**),(**b**)(**2**),(**c**)**3-Form-I**, and d) **3-Form-II**, (compound (**3**) that exists as **Form-I** and **Form-II**)with the thermal ellipsoid of 30% probability.

View Article Online
DOI: 10.1039/D5CE00838G



**Table 2:** Selected torsion angles (°).

| Compounds | (**1**) | (**2**) | (3)-Form-I | (3)-Form-II |
|---|---|---|---|---|
| C6–C1–N1–C7 | 131.9(2) | 156.9(2) | 131.5(2) | 134.1(2) |
| C16–C11–N2–C17 | – | – | –154.6(2) | – |
| C1–N1–C7–C8 | –174.2(2) | –178.7(2) | –177.9(2) | –176.7(2) |
| C11–N2–C17–C18 | – | – | 176.6(2) | – |
| N1–C7–C8–C9 | –130.8(2) | –109.2(2) | –115.6(2) | –118.5(2) |
| N2–C17–C18–C19 | – | – | –115.4(2) | – |
| N1–C7–C8–C10 | 103.5(2) | 125.7(2) | 117.5(2) | 115.7(2) |
| N2–C17–C18–C20 | – | – | 118.9(2) | – |

### *Crystal packing and molecular pairs in (1) [2-fluoro-N-(2-fluorophenyl)-2-methylpropanamide]*

Compound (**1**) crystallizes in the orthorhombic non-centrosymmetric space group $P2_12_12_1$ with Z = 4. The asymmetric unit contains two fluorine atoms where one is connected to C8($sp^3$) and the other is substituted at the *ortho*-position of the benzene ring (Figure 1a). Some selected torsion angles, bond lengths, and bond angles are mentioned in Table 2, S1 and S2, respectively. The crystal structure of (**1**) is stabilized through strong hydrogen bonds like N–H···O along with the presence of weak C–H···O and C–H···F hydrogen bonds and further supported by weak C–H···π interactions. Firstly, N–H···O interaction supported by C–H···O and C–H···F interactions, involving H9B, H10B and F2, constitute the most stabilized motif I (I.E. = –37.5 kJ/mol), which assists the molecules to form a molecular chain along *a*-axis through translational symmetry (x–1, y, z). These chains are connected via motif IV (I.E. = –8.4 kJ/mol) where H10C is oriented towards the centroid (Cg1) of the π-ring (Figure 2f), with a hydrogen to centroid distance (H···Cg1) of 2.75Å (Figure 2a). It is observed that the inclusion of strong hydrogen bonds in motif I (Figure 2c) result in significant electrostatic (67%) contributions. Moreover, motif IV is also electrostatic in nature with the contribution of 59% towards the total interaction energy (Table 3). In another substructure, C–H···O interaction assists the molecules to form a dimer (motif II, I.E.= –10.3 kJ/mol). These dimers are connected to each other (red blocks in Figure 2b)) to form an infinite chain along *b*-axis with the utilization of C–H···F interactions, involving H9C and F2 (motif V, I.E.= –7.1 kJ/mol). Consequently,

View Article Online
DOI: 10.1039/D5CE00838G

long infinite chains are connected in an anti-parallel manner, through another C–H···F interaction (green blocks in Figure 2b), including H3 and F1 (motif III, I.E.= –9.9 kJ/mol), and generating a two-dimensional supramolecular structure in *bc*-plane. The partitioning of the energy contribution reveals that motif III, consisting of C($sp^2$)–H···F–C($sp^2$) interaction (Figure 2e), has equal contribution from both electrostatics and dispersion energies (50%) whereas motif V, incorporating C($sp^3$)–H···F–C($sp^3$) interaction (Figure 2g), is dispersive in nature (59%). Moreover, motif II (including C–H···O) and motif VI (including C–H···π/Cg) are both stabilized by dispersion energies, the contribution being 61% and 69% respectively (Figure 2d & 2h).

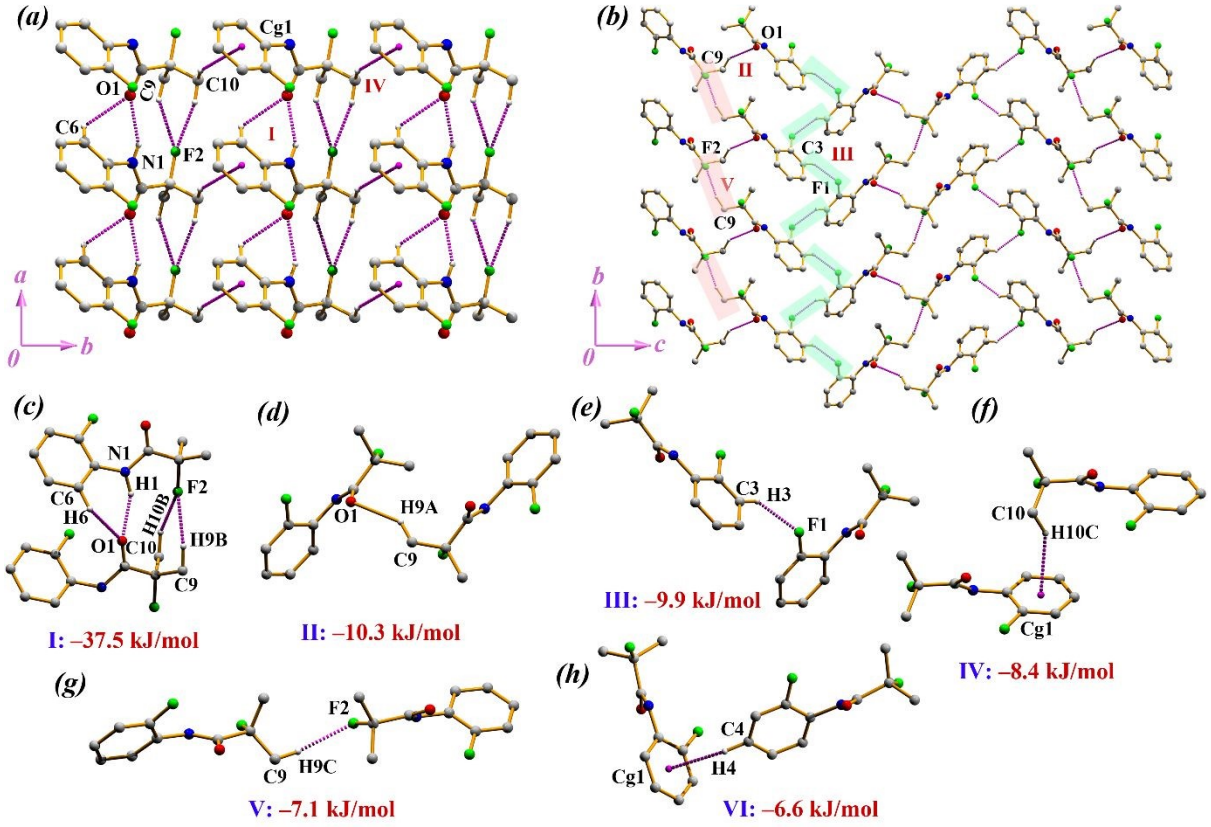


**Figure 2. (a–b)** Crystal packing of (**1**). **(c–h)** Molecular pairs extracted from PIXEL calculation along with their interaction energies in (**1**).

***Crystal packing and molecular pairs in (2) [2-fluoro-N-(3-flurorophenyl)-2-methylpropanamide]***

Compound (**2**) crystallizes in the orthorhombic non-centrosymmetric space group $Pca2_1$ with Z = 4. The asymmetric unit contains one moiety whose benzene ring is substituted with fluorine at *meta*-position (Figure 1b). In the solid-state, the crystal structure is stabilized through like N–H···O, C–H···O, and C–H···F hydrogen bonds. First, the molecules are connected to each

other by N–H···O and C–H···O interactions to form a one-dimensional chain along *c*-axis (motif I, I.E.= –31.7 kJ/mol) generated through the c-glide symmetry (–x+1/2, y, z+1/2). Again, similar molecular chains are connected through C–H···O interaction (motif II, I.E.= –12.9 kJ/mol) with the aid of an *a*-glide plane perpendicular to the crystallographic *b*-axis (Figure 3a). Subsequently, the parallel molecular chains are further connected through C–H···O supported by C–H···F interaction (motif III, I.E.= –11.5 kJ/mol), resulting in a two-dimensional supramolecular arrangement (Figure 3a). It is noted that motif I (Figure 3b), comprising of N–H···O and C–H···O is supported with an additional F···O short contact (2.991(1) Å) and this motif is majorly stabilized by contribution from electrostatics (64%). Although motif II includes short C–H···O interaction, it shows dispersive nature with 58% contribution (Figure 3c).Interestingly, motif III containing C($sp^3$)–H···F–C($sp^3$) and C–H …O=C interaction (Figure 3d), possesses 55% electrostatic energy contribution in the total energy, whereas motif IV stabilized by C($sp^3$)–H···F–C($sp^2$) interaction is dispersive in nature with 60% contribution (Figure 3e).

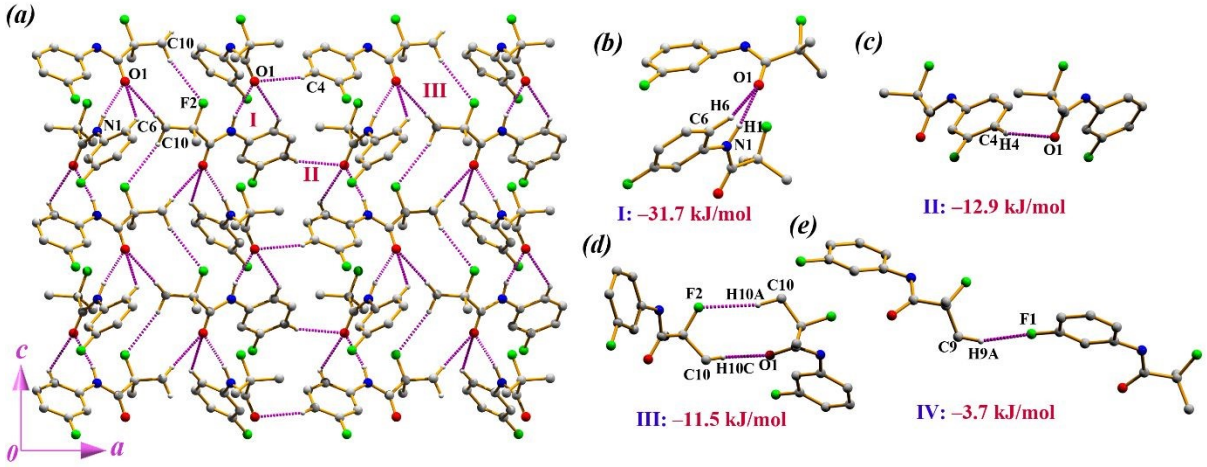


**Figure 3. (a)** Supramolecular self-assembly in (**2**). **(b–e)** All favourable molecular pairs extracted from PIXEL calculation along with their interaction energies in (**2**).

***Crystal packing and molecular pairs in 3-Form-I [2-fluoro-N-(4-fluorophenyl)-2-methylpropanamide]***

Compound (**3**) exhibits structural polymorphism [**3-Form-I** & **3-Form-II**] (Figure 1c & 1d) where the asymmetric units of **I** and **II** contain two and one molecular moieties respectively with the substitution of fluorine atom at the *para*-position in the benzene ring. **3-Form-I** crystallizes in the monoclinic centrosymmetric space group $P2_1/n$ with Z=8, Z′ = 2 and **3-Form-II** crystallizes in the triclinic centrosymmetric space group $P\bar{1}$ with Z = 2, Z′ = 1.

View Article Online
DOI: 10.1039/D5CE00838G

In **3-Form-I**, different crystal packing has been observed incorporating N–H···O along with C–H···O, C–H···F and π–π interaction. In the first substructure depicted in (Figure 4a), moiety A and B together form an infinite molecular chain incorporating N–H···O and C–H···F interactions, involving H2, H19C, H20B, F2 and F4 (motif I, I.E. = –34.3 kJ/mol and motif II, I.E.= –34.2 kJ/mol). The molecular chain propagates along *c*-axis with the symmetry (x–1/2, –y+1/2, z–1/2). The chains are further connected to each other through C–H···F interactions involving H19A, H20C and F1 (motif IX, I.E.= –6.6 kJ/mol), resulting in a two-dimensional supramolecular self-assembly in *ac*-plane. Due to the presence of strong hydrogen bond N–H···O, motif I & II (Figure 5a & 5b) are electrostatic in nature (68% & 65% respectively) whereas motif IX exhibits dispersive nature (53%) consisting of C($sp^3$)–H···F–C($sp^2$) interactions (Figure 5i) with the H…F distances of 2.65 and 2.62 Å. In Figure 4b, C–H···O and C–H···F interactions, involving H10A and F1 in motif III (I.E.= –17.1 kJ/mol) forms a zig-zig molecular chain and these chains are further connected via a centrosymmetric dimeric ring (motif VII, I.E.= –12.5 kJ/mol) consisting of a short C–H···F interaction ($d_{H\cdots F}$= 2.41 Å), thus forming a two-dimensional supramolecular arrangement. In this case, motif III & VII both are electrostatic in nature (66% and 56% respectively) (Figure 5c& 5g). However,motif IV (I.E.= –16.1 kJ/mol) stabilized through C–H···O interaction is connected to each other via C–H···F interactions (motif VI, I.E.= –12.6 kJ/mol and motif VIII, I.E.= –10.9 kJ/mol), forming a two-dimensional supramolecular network (Figure 4c). The motif IV is dispersive in nature (59%) (Figure 5d) whereas motif VI consisting of short C($sp^2$)–H···F–C($sp^2$) interactions ($d_{H\cdots F}$= 2.43 Å and 2.39 Å) is stabilized by electrostatic energy (65%) (Figure 5f). Moreover, motif VIII includes a π–π interaction (Cg1–Cg2) with a centroid separation of 4.197(2) Å along with the C($sp^3$)–H···F–C($sp^2$) interactions (Figure 5h), having a higher dispersion energy (60%) contribution.Lastly, motif V (I.E. = –12.8 kJ/mol) and motif X (I.E.= – 6.2 kJ/mol) are stabilized by H…H short contacts (Figure 5e & 5j) and these are dispersive in nature with the contribution of 73% and 84% respectively.

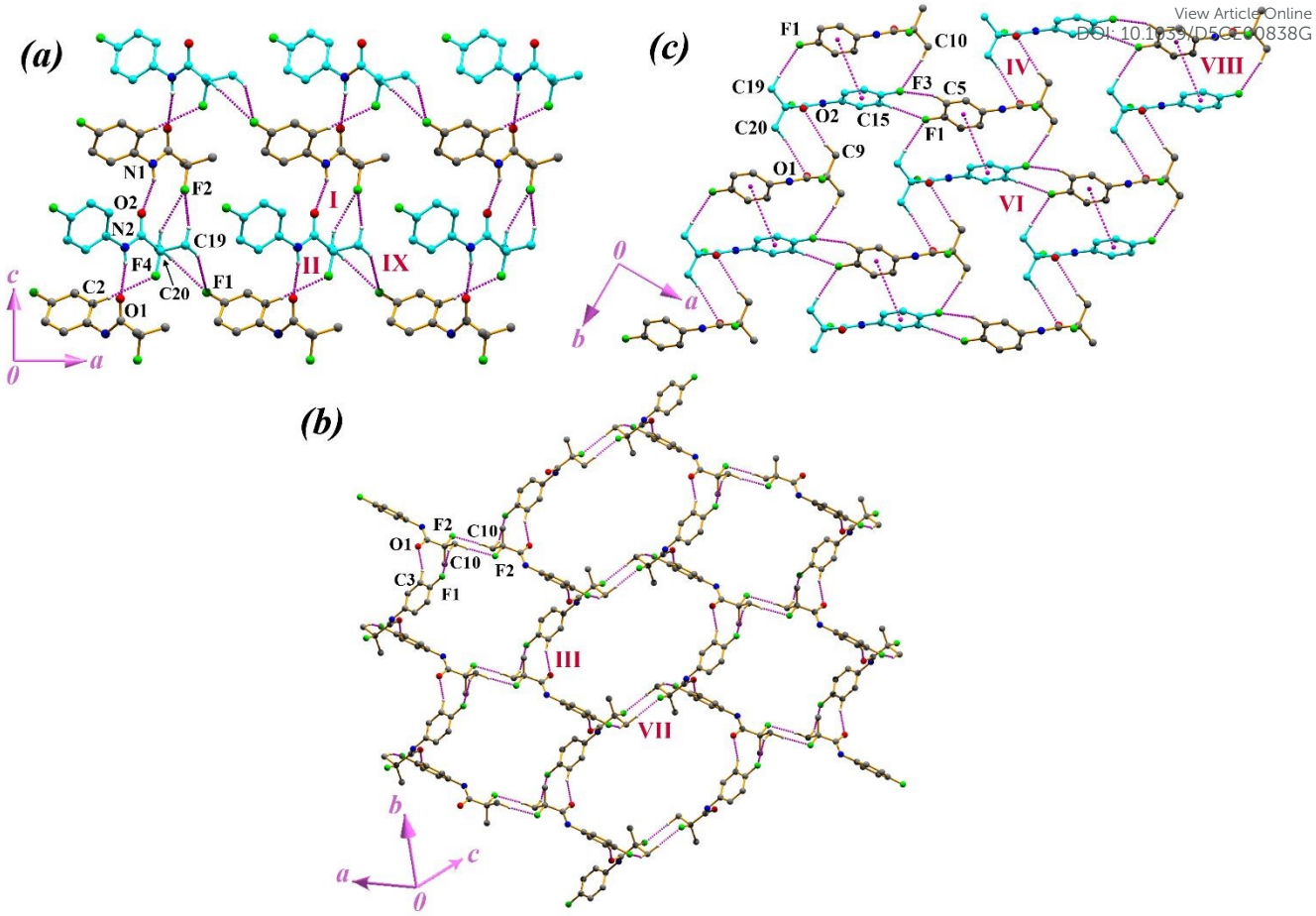


**Figure 4. (a-c)** Supramolecular self-assemblies in **3-Form-I**. The carbon atoms are deep grey in moiety A and turquoise blue in moiety B.

View Article Online
DOI: 10.1039/D5CE00838G

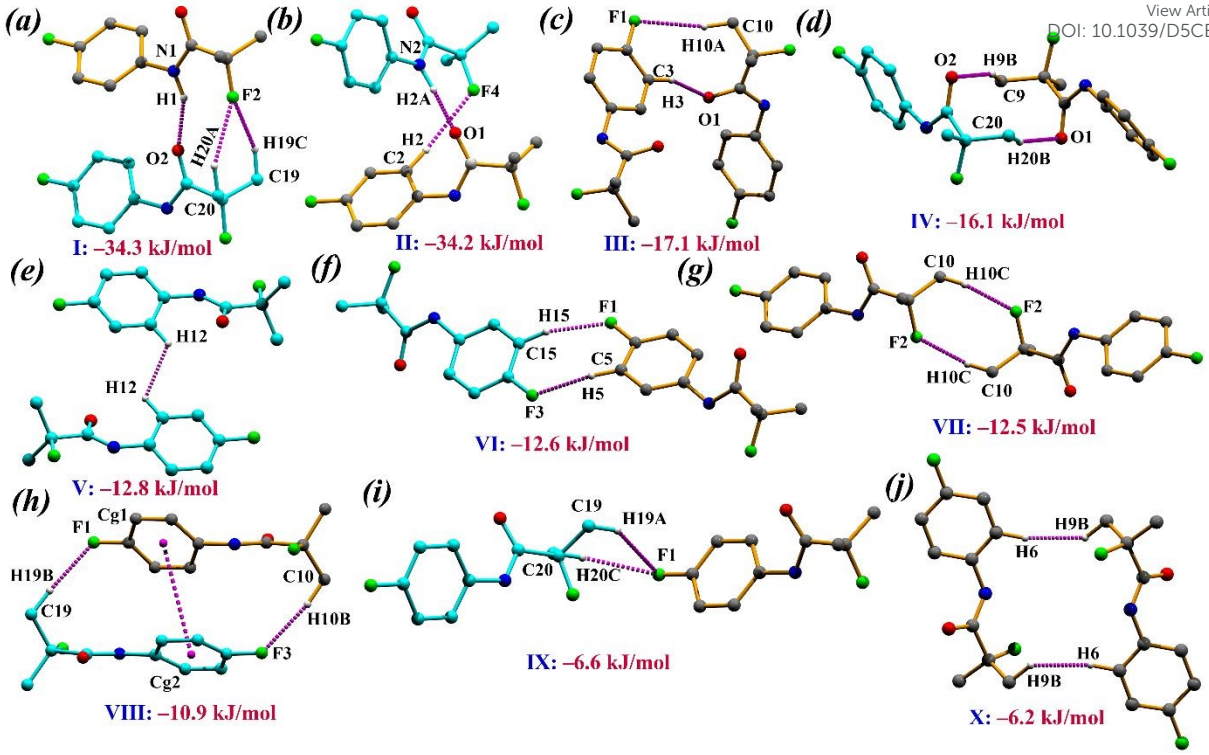


**Figure 5. (a–j)** Molecular pairs in **3-Form-I** extracted from PIXEL calculation along with their interaction energies. The carbon atoms are deep grey in moiety A and turquoise blue in moiety B.

***Crystal packing and molecular pairs in 3-Form-II [2-fluoro-N-(4-fluorophenyl)-2-methylpropanamide]***

In **3-Form-II**, the molecules are arranged in the solid-state through N–H···O, C–H···O and C–H···F interactions. Firstly, N–H···O in association with C–H···O and C–H···F interaction, involving H9B, H10B and F2, forms an infinite molecular chain (motif I, I.E.= –28.5 kJ/mol) involving the translational symmetry (x–1, y, z). Next, two such chains are connected to each other via a centrosymmetric dimeric ring stabilized by C–H···F interaction (motif IV, I.E.= –13.7 kJ/mol) and generated through the inversion symmetry (–x, –y, –z+1), resulting in another infinite molecular chain. These molecular chains are further connected to each other (Figure 6a) via a centrosymmetric dimeric ring containing C–H···F interaction (motif V, I.E.= –10.6 kJ/mol) (Figure 6g). It is observed that motif I (Figure 6c), containing strong N–H···O hydrogen bond, is electrostatic in nature (67%). Importantly, motif IV (Figure 6f) exhibits electrostatic nature (65%) involving short C($sp^2$)–H···F–C($sp^2$) interaction ($d_{H\cdots F}$= 2.39 Å) whereas, motif V consisting of C($sp^3$)–H···F–C($sp^3$) interaction ($d_{H\cdots F}$= 2.49 Å), also shows electrostatic nature with less contribution (51%) compared to IV. In another substructure, the alternative association of C–H···O (motif II, I.E.= –17.1 kJ/mol) and C–H···F interaction

View Article Online
DOI: 10.1039/D5CE00838G

(motif III, I.E.= –15.0 kJ/mol) helps the molecules to assemble in an infinite molecular chain generated by the symmetry (–x+1, –y+1, –z) and (–x, –y+1, –z+1) respectively. These parallel chains are connected to each other via motif V, resulting in a two-dimensional supramolecular assembly in *bc*-plane (Figure 6b). However, motif II comprising C–H···O, and motif III comprising C($sp^3$)–H···F–C($sp^2$) interaction, contribute more to the dispersion energy (58% and 66% respectively) in comparison to other motifs (Figure 6d & 6e).

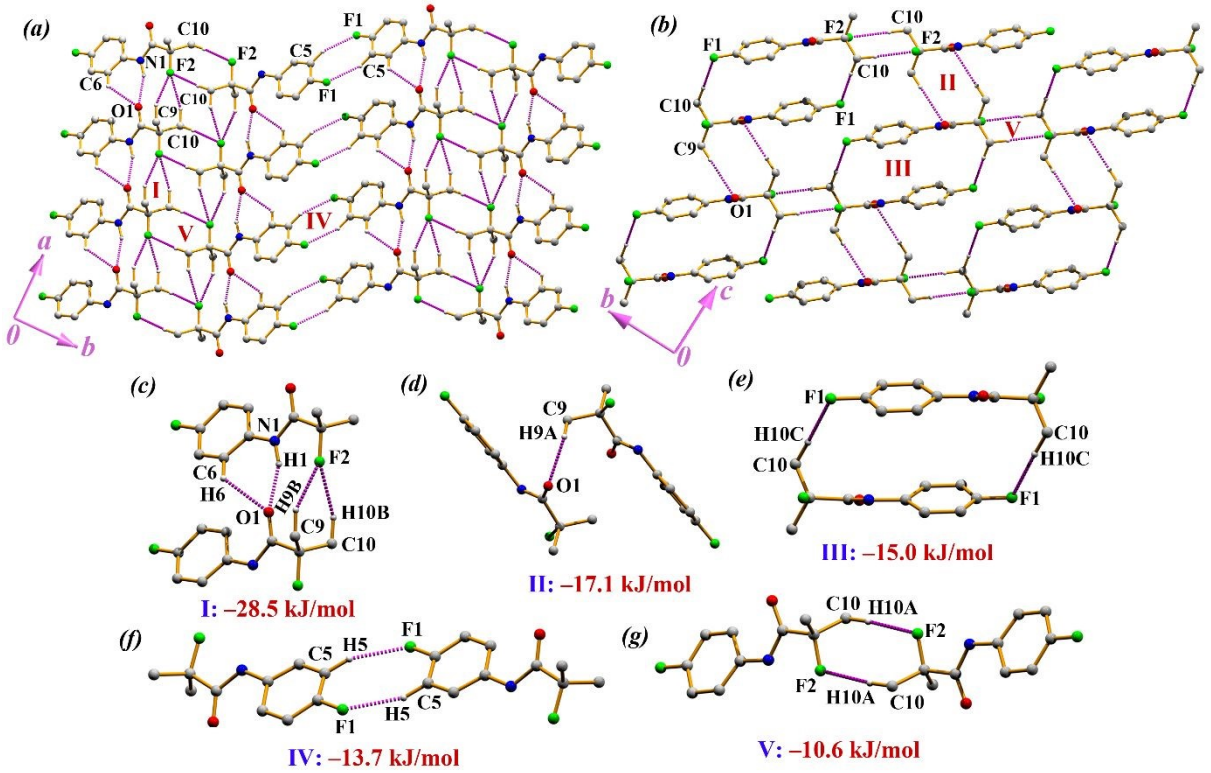


**Figure 6. (a-b)** Supramolecular packing in **3-Form-II**. **(c–g)** Molecular pairs extracted from PIXEL calculation along with their interaction energies in **3-Form-II**.

**Table 3.** Interaction energies (kJ/mol) of the molecular pairs/motifs of compounds (**1–2**) and **3-Form-I** and **3-Form-II**. The distances are neutron normalized.

| Motifs | Symmetry Code | Cg···Cg | $E_{Coul}$ | $E_{Pol}$ | $E_{Disp}$ | $E_{Rep}$ | $E_{tot}$ | Involved interactions[a] | Geometry (Å/°) D···A, H···A, ∠D–H···A |
|---|---|---|---|---|---|---|---|---|---|
| **(1)** | | | | | | | | | |
| **I** | (x–1, y, z) | 5.113 | –48.9 | –15.2 | –31.2 | 57.8 | –37.5 | C6–H6···O1 | 3.223(2), 2.48, 125 |
| | | | | | | | | N1–H1···O1 | 2.976(2), 2.05, 148 |
| | | | | | | | | C10–H10B···F2 | 3.343(2), 2.36, 150 |
| | | | | | | | | C9–H9B···F2 | 3.465(2), 2.57, 140 |

View Article Online
DOI: 10.1039/D5CE00838G

| | | | | | | | | | |
|---|---|---|---|---|---|---|---|---|---|
| **II** | (x–1/2, –y+1/2, –z+1) | 6.747 | –6.7 | –3.3 | –15.5 | 15.3 | –10.3 | C9–H9A···O1 | 3.505(2), 2.55, 147 |
| **III** | (–x, y+1/2, –z+1/2) | 8.646 | –7.7 | –2.1 | –9.8 | 9.7 | –9.9 | C3–H3···F1 | 3.190(2), 2.35, 134 |
| **IV** | (x, y–1, z) | 6.775 | –8.1 | –3.4 | –16.3 | 19.5 | –8.4 | C10–H10C···Cg1 | 3.707(2), 2.75, 146 |
| **V** | (x+1/2, –y+3/2, –z+1) | 9.434 | –5.9 | –2.0 | –11.5 | 12.3 | –7.1 | C9–H9C···F2 | 3.500(2), 2.51, 152 |
| **VI** | (–x+1, y–1/2, –z+1/2) | 8.466 | –3.9 | –2.0 | –12.9 | 12.2 | –6.6 | C4–H4···Cg1 | 3.834(2), 2.85, 150 |
| **(2)** | | | | | | | | | |
| **I** | (–x+1/2, y, z+1/2) | 4.356 | –46.9 | –16.0 | –34.8 | 66.0 | –31.7 | N1–H1···O1<br>C6–H6···O1 | 2.953(2), 1.96, 162<br>3.255(3), 2.48, 128 |
| **II** | (x–1/2, –y+2, z) | 7.789 | –9.8 | –4.1 | –19.4 | 20.4 | –12.9 | C4–H4···O1 | 3.396(3), 2.47, 144 |
| **III** | (–x, –y+1, z–1/2) | 8.374 | –9.7 | –2.8 | –10.3 | 11.3 | –11.5 | C10–H10C···O1<br>C10–H10A···F2 | 3.561(3), 2.51, 166<br>3.773(3), 2.72, 166 |
| **IV** | (–x+1/2, y–1, z+1/2) | 10.416 | –2.8 | –1.0 | –5.7 | 5.8 | –3.7 | C9–H9A···F1 | 3.284(3), 2.58, 122 |
| **3-Form-I** | | | | | | | | | |
| **I (AB)** | (x–1/2, –y+1/2, z–1/2) | 5.172 | –46.2 | –14.5 | –28.9 | 55.4 | –34.3 | N1–H1···O2<br>C19–H19C···F2<br>C20–H20A···F2 | 2.871(2), 1.95, 148<br>3.558(2), 2.62, 145<br>3.524(2), 2.57, 147 |
| **II (AB)** | (x, y, z) | 4.803 | –34.6 | –12.0 | –25.5 | 37.9 | –34.2 | N2–H2···O1<br>C2–H2···F4 | 2.992(1), 2.05, 151<br>3.813(2), 2.75, 167 |
| **III (AA)** | (–x+3/2, y–1/2, –z+1/2) | 7.392 | –21.4 | –7.8 | –15.2 | 27.4 | –17.1 | C10–H10A···F1<br>C3–H3···O1 | 3.929(2), 2.90, 160<br>3.244(2), 2.20, 161 |
| **IV (AB)** | (–x+3/2, y–1/2, –z+1/2) | 5.417 | –12.5 | –4.2 | –23.6 | 24.2 | –16.1 | C9–H9B···O2<br>C20–H20B···O1 | 3.733(2), 2.70, 159<br>3.797(2), 2.75, 163 |
| **V (BB)** | (–x+2, –y, –z+1) | 6.449 | –4.5 | –3.2 | –20.6 | 15.4 | –12.8 | H12···H12 | 2.32 |
| **VI (AB)** | (–x+1/2, y+1/2, –z+1/2) | 11.937 | –12.7 | –2.3 | –8.1 | 10.5 | –12.6 | C5–H5···F3<br>C15–H15···F1 | 3.437(2), 2.43, 155<br>3.444(2), 2.39, 165 |

| | | | | | | | | | |
|---|---|---|---|---|---|---|---|---|---|
| **VII (AA)** | (–x+2, –y, –z) | 9.156 | –12.7 | –2.7 | –12.3 | 15.2 | –12.5 | C10–H10C···F2 | 3.474(2), 2.41, 170 |
| **VIII (AB)** | (–x+3/2, y+1/2, –z+1/2) | 5.846 | –14.8 | –5.3 | –30.6 | 39.8 | –10.9 | C10–H10B···F3<br>Cg1···Cg2<br>C19–H19B···F1 | 3.616(2), 2.56, 167<br>4.197(2)<br>3.544(2), 2.47, 171 |
| **IX (AB)** | (x–1, y, z) | 9.627 | –5.5 | –1.3 | –7.6 | 7.9 | –6.6 | C20–H20C···F1<br>C19–H19A···F1 | 3.591(2), 2.65, 145<br>3.567(2), 2.62, 146 |
| **X (AA)** | (–x+1, –y, –z) | 6.312 | 0.0 | –2.4 | –12.4 | 8.6 | –6.2 | H9B···H6 | 2.32 |
| **3-Form-II** | | | | | | | | | |
| **I** | (x–1, y, z) | 5.180 | –63.7 | –21.7 | –42.8 | 99.7 | –28.5 | C6–H6···O1<br>N1–H1···O1<br>C10–H10B···F2<br>C9–H9B···F2 | 3.177(4), 2.42, 126<br>2.954(2), 2.02, 150<br>3.502(2), 2.57, 144<br>3.458(3), 2.50, 148 |
| **II** | (–x+1, –y+1, –z) | 5.307 | –12.8 | –4.0 | –23.1 | 22.7 | –17.1 | C9–H9A···O1 | 3.783(3), 2.73, 165 |
| **III** | (–x, –y+1, –z+1) | 5.731 | –8.9 | –2.8 | –22.7 | 19.5 | –15.0 | C10–H10C···F1 | 3.546(2), 2.48, 167 |
| **IV** | (–x, –y, –z+1) | 11.908 | –13.9 | –2.6 | –8.9 | 11.7 | –13.7 | C5–H5···F1 | 3.418(5), 2.39, 160 |
| **V** | (–x, –y+2, –z) | 9.299 | –9.7 | –2.4 | –11.6 | 13.2 | –10.6 | C10–H10A···F2 | 3.566(2), 2.49, 175 |

[a]Cg1 is the centroid of the π- ring (C1–C6) in (**1**) and **3-Form-I** and Cg2 is the centroid of the π- ring (C11–C16) in **3-Form-I**.

***Lattice Energy***

The total lattice energy for (**1**–**2**) and **3-Form-I**and **3-Form-II** are also calculated from PIXEL calculation depicted in Table 4. The highest Coulombic energy is possessed by **3-Form-II** (–89.9 kJ/mol) and lowest by (**2**) (–71.7 kJ/mol). The cell dipole contribution of –3.1 kJ/mol appears in (**2**) due to the association with a polar space group. The contribution of dispersion energy is highest for (**2**) (52%). Moreover, the total lattice energy is occupied by (**1**) with a value of –87.8 kJ/mol.

**Table 4.** Lattice energy (kJ/mol) for (**1**–**2**),**3-Form-I** and**3-Form-II**.

| **Compounds** | $E_{Coul}$ | $E_{Pol}$ | $E_{Disp}$ | $E_{Rep}$ | $E_{cd}$ | $E_{Tot}$ |
|---|---|---|---|---|---|---|
| (**1**) | –83.8 | –27.2 | –109.5 | 132.7 | 0.0 | –87.8 |
| (**2**) | –71.7 | –24.8 | –103.0 | 125.2 | –3.1 | –77.4 |

View Article Online
DOI: 10.1039/D5CE00838G

| | | | | | | |
|---|---|---|---|---|---|---|
| **3-Form-I** | –79.1 | –26.4 | –100.7 | 123.3 | 0.0 | –82.8 |
| **3-Form-II** | –89.9 | –30.1 | –106.6 | 152.6 | 0.0 | –74.0 |

***Hirshfeld Surface Analysis***

The Hirshfeld surface analysis has been carried for all compounds to characterize the intermolecular interactions controlling the crystal structures and the favourable molecular dimers. The Hirshfeld surfaces are mapped over $d_{norm}$, shape index and curvedness (Figure S5) where the feasible hydrogen bonds are visualized as bright-red spots on $d_{norm}$ surface and π–π interaction is visible by red-blue triangle on shape index and flat region on curvedness surface. The intense bright red spots indicate the presence of N–H··O interaction in all compounds. The less bright-red spots on the surface near fluorine atoms characterizing them as a contributor to the weak hydrogen bonds. As on **3-Form-I** contains π-π interaction in the packing, a red-blue triangle and a flat region are evidenced on shape index and curvedness respectively (Figure S5c).

Additionally, 2D fingerprint plots (Figure 7) of all compounds are studied to quantify the percentage contribution of each probable contacts occurring in the crystal structures. All the decomposed fingerprint plots are depicted in Figure S6–S9. The significant contribution of F···H/H···F contacts is observed in all compounds and its contribution ranges from 20.8% to 25.2% which denotes more contribution than O···H/H···O contacts ranging from 9.4% to 11.5%). In (**1**) C–H···π is evidenced from the wings appeared in the decomposed fingerprint plot for C···H/H···C contact. In (**2**) and **3-Form-I**, the contribution of F···O/O···F contacts are also observed with the contribution of 0.8% and 0.3% respectively. The highest contribution for C···F/F···C contacts is 6.1% in (**2**) amongst all compounds. Similarly, as most favourable centrosymmetric dimers incorporating C–H···F interaction have been found in **3-Form-I** (A & B) and **II**, the highest contribution for F···H/H···F contacts has been availed by the polymorphs with the contribution of 25.2%, 24.3%, and 23.3%. Moreover, **3-Form-I** (A&B) and **II** reveals the existence of F···F contacts with the contribution of 0.2%,1.4%, and 1.3% respectively whereas there are no such contacts found in compound (**1**–**2**). The percentage contribution of the contacts in all compounds is shown in a bar graph (Figure 8).

View Article Online
DOI: 10.1039/D5CE00838G



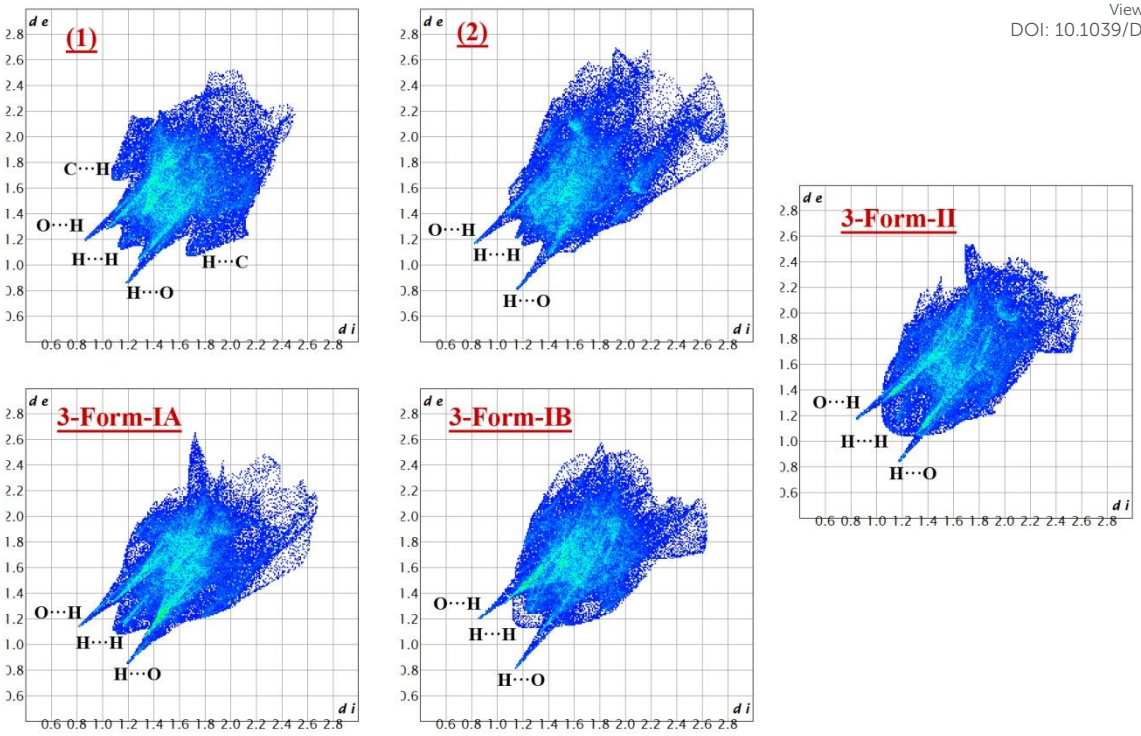


**Figure 7.** 2D fingerprint plots for all contacts observed in all compounds.

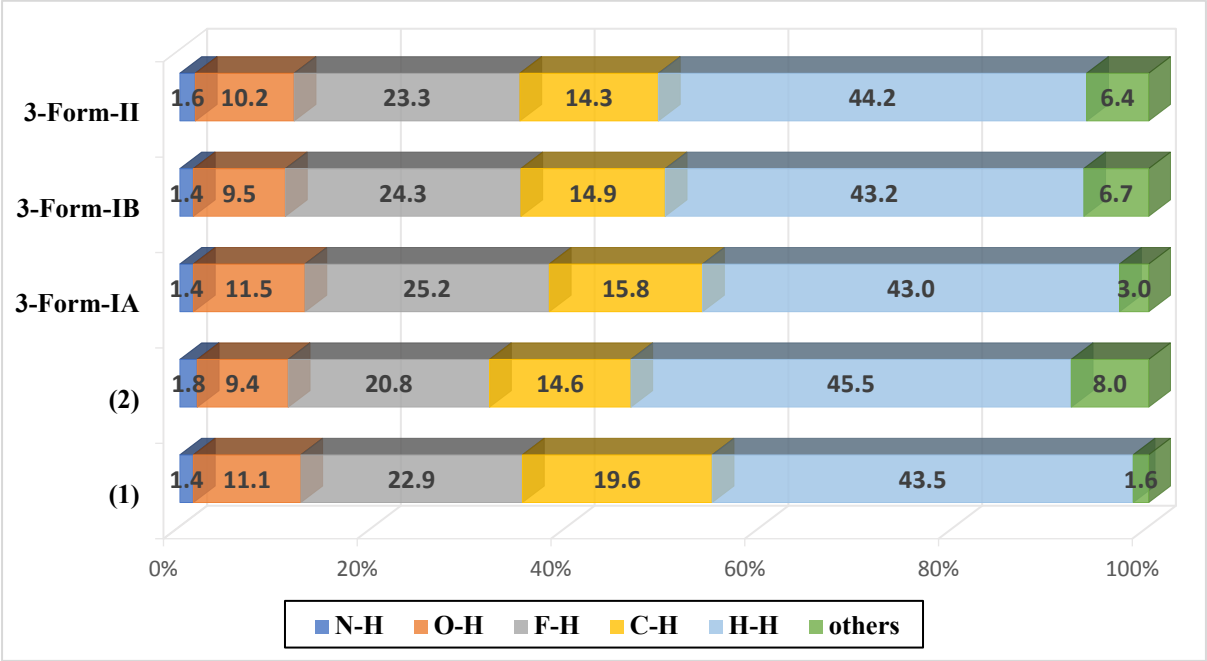


**Figure 8.** Percentage contributions of various contacts to the Hirshfeld surface area in all four compounds.

### *Analysis from Quantum Theory of Atoms in Molecules*

Topological analysis based on the electron density distribution, has been performed for C–H···F interactions observed in these compounds. The existence of (3, –1) bond critical points

View Article Online
DOI: 10.1039/D5CE00838G



(BCPs) and associated bond paths characterize these contacts at their crystal geometry. The results are tabulated in Table 5 for C–H···F interactions only and the topological parameters of other interactions in the selected motifs are listed in Table S4. It is of interest to study the order of the strength of C–H···F bonds in terms of the hybridization of the carbon atom attached to hydrogen and the fluorine atoms. We have categorized these interactions into four classes in terms of the hybridization of the carbon atom, i.e., C($sp^3$)–H···F–C($sp^3$), C($sp^2$)–H···F–C($sp^3$),C($sp^3$)–H···F–C($sp^2$), and C($sp^2$)–H···F–C($sp^2$). A total of seven motifs featuring C($sp^3$)–H···F–C($sp^3$) interaction (Figure 9a, 9c, 9d, 9f, 9j, 9m & 9p) has been observed in which the hydrogen atom bonded to an $sp^3$–hybridized carbon, acts as a donor to the fluorine atom which is also attached to an $sp^3$ hybridized carbon. The electron density at bond critical point (BCP) varies from 0.0297 to 0.0622 e/Å$^3$ corresponding to the bond dissociation energy ranging from 3.5578 to 8.4336 kJ/mol. The highest electron density at BCP of C($sp^3$)–H···F–C($sp^3$) interaction is exhibited by motif I in (**1**) (Figure 9a). The corresponding Laplacian of charge densities ($\nabla^2(\rho)$) ranges from 0.4056 to 0.8377 e/Å$^5$.

Next, C($sp^2$)–H···F–C($sp^3$) interaction is present in motif II of **3-Form-I** only (Figure 9g). The electron density at BCP of C2–H2···F4 interaction (motif II in **3-Form-I**) acquires a value of 0.0277 eÅ$^{-3}$ while the corresponding Laplacian and dissociation energy values are 0.3790 eÅ$^{-5}$ and 3.2945 kJ/mol, respectively. These values are considerably lower in magnitude compared to those of above-mentioned C($sp^3$)–H···F–C($sp^3$) interactions.

Subsequently, the focus is on the other two classes of C–H···F interactions (C($sp^3$)–H···F–C($sp^2$) and C($sp^2$)–H···F–C($sp^2$)) involving the fluorine atom attached to $sp^2$ carbon atom of the aryl ring. To analyse the topological parameters for C($sp^3$)–H···F–C($sp^2$) interaction, five motifs have been considered (Figure 9e, 9h, 9k, 9l & 9n). The electron density at BCP ranges from a minimum of 0.0203 eÅ$^{-3}$ (C10–H10A···F1 in **3-Form-I**, Figure 9h) to a maximum of 0.0514 eÅ$^{-3}$ (C19–H19B···F1 in **3-Form-I**, Figure 9k). These interactions reveal the corresponding Laplacian of electron density in the range of 0.2945 and 0.6494 eÅ$^{-5}$ and dissociation energy between 2.3722 kJ/mol to 6.5890 kJ/mol.

Lastly, there are only three motifs which are stabilized by C($sp^2$)–H···F–C($sp^2$) interaction (Figure 9b, 9i & 9o). The electron density lies in a comparatively elevated range of 0.0541eÅ$^{-3}$ (C15–H15···F1 in **3-Form-I**, Figure 9i) to 0.0608 eÅ$^{-3}$ (C3–H3···F1 in (**1**), (Figure 9b) corresponding to stronger interactions than other three classes. The dissociation energy values, ranging from 6.9842 kJ/mol to 8.8292 kJ/mol, also suggest a relatively strong bond strength.

View Article Online
DOI: 10.1039/D5CE00838G

Moreover, the Laplacian of electron density acquires the highest value of 1.3639 eÅ$^{-5}$ and the lowest value of 0.7097 eÅ$^{-5}$.

A comparison of all the topological parameters, and their detailed analysis suggest that the presence of C($sp^3$)−H···F−C($sp^3$) and C($sp^2$)−H···F−C($sp^2$) interactions acquire higher stabilization in comparison to the C($sp^3$)−H···F−C($sp^2$) and C($sp^2$)−H···F−C($sp^3$)interactions. Similar observations have also been made in the previous study done by Panini *et al.*.[10]. Moreover, the range of $\rho$ value, positive value of Laplacian of $\rho[\nabla^2(\rho) > 0]$ and $\left|\frac{V(r)}{G(r)}\right| < 1$ at BCPs, confirm the bonding nature of these hydrogen bonds and establish theseto be closed shell interactions. Furthermore, the variation of electron density at BCP and Laplacian of electron density with the bond path length of H···F contacts has been shown (Figure S10).

View Article Online
DOI: 10.1039/D5CE00838G



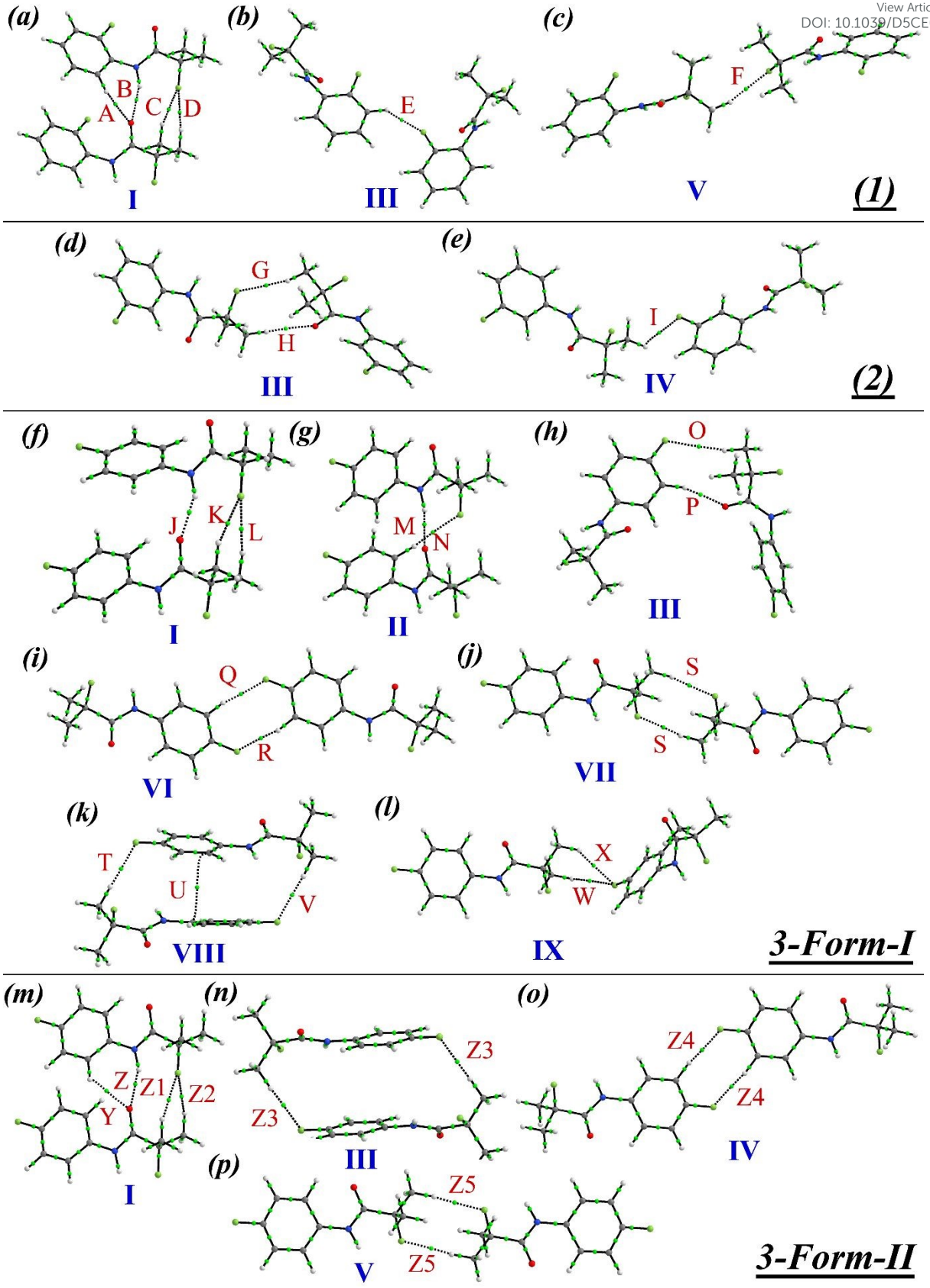

View Article Online
DOI: 10.1039/D5CE00838G

**Figure 9.** Distribution of bond critical points (BCP) and bond paths of intermolecular interactions in the molecular pairs involving C–H···F interactions in **(a–c)** (**1**), **(d–e)** (**2**), **(f–l)3-Form-I**, and**(m–p) 3-Form-II** respectively.

**Table 5.** Analysis of topological parameters of intermolecular C–H···F interactions in compounds (**1**–**2**), **3-Form-I** &**II**.

| Compound | Motif | $\rho(r)$ (eÅ$^{-3}$) | $\nabla^2(\rho)$ (eÅ$^{-5}$) | $V(r)$ (a.u.) | $G(r)$ (a.u.) | $H(r)$ (a.u.) | $\left\|\frac{V(r)}{G(r)}\right\|$ | $D_e$ (kJ/mol) |
|---|---|---|---|---|---|---|---|---|
| **C($sp^3$)−H···F−C($sp^3$)** | | | | | | | | |
| (**1**) | I (C) | 0.0622 | 0.8377 | −0.0064 | 0.0075 | 0.0011 | 0.8533 | 8.4336 |
| | (D) | 0.0412 | 0.5673 | −0.0041 | 0.0050 | 0.0009 | 0.8200 | 5.4029 |
| | V (F) | 0.0500 | 0.6421 | –0.0049 | 0.0058 | 0.0009 | 0.8448 | 6.4575 |
| (**2**) | III (G) | 0.0297 | 0.4056 | −0.0027 | 0.0035 | 0.0008 | 0.7714 | 3.5578 |
| **3-Form-I** | I (K) | 0.0399 | 0.5480 | −0.0040 | 0.0048 | 0.0008 | 0.8333 | 5.2710 |
| | (L) | 0.0358 | 0.4973 | −0.0035 | 0.0043 | 0.0008 | 0.8140 | 4.6120 |
| | VII (S) | 0.0608 | 0.7677 | −0.0060 | 0.0070 | 0.0010 | 0.8571 | 7.9065 |
| **3-Form-II** | I (Z1) | 0.0460 | 0.6301 | −0.0046 | 0.0056 | 0.0010 | 0.8214 | 6.0619 |
| | (Z2) | 0.0399 | 0.5552 | −0.0040 | 0.0049 | 0.0009 | 0.8163 | 5.2710 |
| | V (Z5) | 0.0514 | 0.6445 | −0.0049 | 0.0058 | 0.0009 | 0.8448 | 6.4571 |
| **C($sp^2$)−H···F−C($sp^3$)** | | | | | | | | |
| **3-Form-I** | II (N) | 0.0277 | 0.3790 | −0.0025 | 0.0032 | 0.0007 | 0.7813 | 3.2945 |
| **C($sp^3$)−H···F−C($sp^2$)** | | | | | | | | |
| (**2**) | IV (I) | 0.0453 | 0.6276 | −0.0046 | 0.0055 | 0.0009 | 0.8364 | 6.0619 |
| **3-Form-I** | III (O) | 0.0203 | 0.2945 | −0.0018 | 0.0024 | 0.0006 | 0.7500 | 2.3722 |
| | VIII (T) | 0.0514 | 0.6494 | −0.0050 | 0.0058 | 0.0008 | 0.8621 | 6.5890 |
| | (V) | 0.0426 | 0.5504 | −0.0041 | 0.0049 | 0.0008 | 0.8367 | 5.4029 |
| | IX (W) | 0.0331 | 0.4659 | −0.0033 | 0.0041 | 0.0008 | 0.8049 | 4.3487 |
| | (X) | 0.0399 | 0.5287 | −0.0039 | 0.0047 | 0.0008 | 0.8298 | 5.1391 |
| **3-Form-II** | III (Z3) | 0.0507 | 0.6397 | −0.0049 | 0.0058 | 0.0009 | 0.8448 | 6.4571 |

View Article Online
DOI: 10.1039/D5CE00838G

| | | | | | | | | |
|---|---|---|---|---|---|---|---|---|
| | | | | **C($sp^2$)−H···F−C($sp^2$)** | | | | |
| (**1**) | III (E) | 0.0608 | 1.3639 | −0.0067 | 0.0104 | 0.0037 | 0.6442 | 8.8292 |
| **3-Form-I** | VI (Q)<br>(R) | 0.0541<br>0.0575 | 0.7097<br>0.7556 | −0.0053<br>−0.0056 | 0.0063<br>0.0067 | 0.0010<br>0.0011 | 0.8413<br>0.8358 | 6.9842<br>7.3794 |
| **3-Form-II** | IV (Z4) | 0.0575 | 0.7749 | −0.0058 | 0.0069 | 0.0011 | 0.8406 | 7.6432 |

### *Conclusions*

The present investigation depicts the role of weak C–H···F interactions in addition to strong H-bonds. The pertinent contribution of organic fluorine attached to two different hybridized carbon atoms ($sp^3$/$sp^2$) has been analysed in terms of their reoccurrence in structural motifs in the presence of strong hydrogen bonds. The intermolecular interactions co-exist in the crystal packing and play the role of secondary interactions in the formation of different supramolecular structures. The combined contribution of different interactions towards the formation of different supramolecular motifs was quantified from PIXEL. Topological parameters characterized via QTAIM method establish that individual interactions that constitute these supramolecular motifs are closed-shell interactions. Henceforth, it would be of interest to study the impact of the hybridization of carbon atom ($sp^3$/$sp^2$) with a greater number of fluorine atoms on the aryl framework towards the overall stabilization of the crystal structures. Futuristic studies will be directed towards such investigations.

### *Acknowledgements*

PD gratefully acknowledges the Department of Science and Technology (Govt. of India) for DST-Inspire fellowship (DST/INSPIRE Fellowship/2019/IF190666). The authors thank IISER Bhopal for research facilities and infrastructure.

### *Conflict of Interest*

The authors declare no conflict of interest.

### *References*

1 D. Chopra and T. N. Guru Row, Role of organic fluorine in crystal engineering, *CrystEngComm*, 2011, **13**, 2175–2186.

2 M. Inoue, Y. Sumii, N. Shibata, Contribution of Organofluorine Compounds to Pharmaceuticals, *ACS Omega*, 2020, **5**, 10633–10640.

3 P. Panini and D. Chopra, Experimental and Theoretical Characterization of Short Hal-Bonds with Organic Fluorine in Molecular Crystals, *Cryst. Growth Des.*,2014, **14**, 7, 3155–3168.

4 H. J. Schneider, Hydrogen bonds with fluorine. Studies in solution, in gas phase and by computations, conflicting conclusions from crystallographic analyses, *Chem. Sci.*, 2012, **3**, 1381–1394.

5 G. R. Desiraju, A Bond by Any Other Name, *Angew. Chem. Int. Ed.*, 2011, **50**, 52–59.

6 C. Dalvit, C. Invernizzi and A. Vulpetti, Fluorine as a Hydrogen-Bond Acceptor: Experimental Evidence and Computational Calculations, *Chem. Eur. J.*, 2014, **20**, 11058–11068.

7 M. R. Sarkar and D. Chopra, Evolution in the Understanding of Noncovalent Interactions Involving Fluorine: From Inception to Maturity to Properties, *Cryst. Growth Des.*, 2024, **24**, 8674–8687.

8 L. Singla, H. R. Yadav and A. R. Choudhury, Structural and Computational Analysis of Organic Fluorine-Mediated Interactions in Controlling the Crystal Packing of Tetrafluorinated Secondary Amides in the Presence of Weak C–H···O=C Hydrogen Bonds, *Cryst. Growth Des.*, 2022, **22**, 1604–1622.

9 P. Das, G. B. D. Rao, S. Bhandary, K. Mandal, S. K. Seth and D. Chopra, Quantitative Investigation into the Role of Intermolecular Interactions in Crystalline Fluorinated Triazoles, *Cryst. Growth Des.*, 2024, **24**, 703–721.

10 P. Panini, R. G. Gonnade and D. Chopra, Experimental and computational analysis of supramolecular motifs involving $C_{sp}^2$(aromatic)–F and $CF_3$ groups in organic solids, *New J. Chem.*,2016, **40**, 4981–5001.

11 P. Panini and D. Chopra, Experimental and computational insights into the nature of weak intermolecular interactions in trifluoromethyl-substituted isomeric crystalline *N*-methyl-*N*-phenylbenzamides, *New J. Chem.*,2015, **39**, 8720–8738.

12 C. R. Pitts, M. A. Siegler and T. Lectka, Intermolecular Aliphatic C–F···H–C Interaction in the Presence of "Stronger" Hydrogen Bond Acceptors: Crystallographic, Computational, and IR Studies, *J. Org. Chem.*, 2017, **82**, 3996–4000.

13 D. Dey and D. Chopra, Evaluation of the Role of Isostructurality in Fluorinated Phenyl Benzoates, *Cryst. Growth Des.*, 2017, **17**, 5117–5128.

14 D. Dey, S. K. Seth, T. P. Mohan and D. Chopra, Quantitative analysis of intermolecular interactions in crystalline substituted triazoles, *J. Mol. Struct.*, 2023, **1273**, 134380.

15 A. Hasija and D. Chopra, Concomitant dimorphism in diphenyl (3, 4–difluorophenyl) phosphoramidates, *Acta Crystallogr A Found Adv*, 2017, **73**, C782–C782.

16 A. Hasija, R. Bhowal and D. Chopra, Quantitative investigation of weak intermolecular interactions of –F and $–CF_3$ substituted *in situ* cryocrystallized benzaldehydes, *Cryst. Growth Des.*, 2020, **20**, 7921–7933.

17 P. Panini and D. Chopra, Role of intermolecular interactions involving organic fluorine in trifluoromethylated benzanilides, *CrystEngComm*, 2014, **14**, 1972–1989.

18 P. Panini and D. Chopra, Quantitative insights into energy contributions of intermolecular interactions in fluorine and trifluoromethyl substituted isomeric *N*-phenylacetamides and *N*-methylbenzamides, *CrystEngComm*, 2013, **15**, 3711–3733.

19 P. Dey, R. Bhowal, S. K. Seth and D. Chopra, Understanding the Nature and Energetics of C–H···F Interactions in Crystalline Propanamides, *Cryst. Growth Des.*, 2025, **25**, 4263–4282.

20 Bruker, *APEX2*; Bruker AXS Inc.: Madison, Winconsin, USA, 2012.

21 *SAINT and SADABS*, Bruker AXS Inc. Madison, Wisconsin, USA, 2008.

22 Sheldrick, G.M. A short history of SHELX. *Acta Cryst. A*,2008, **64**, 112–122.

23 Sheldrick, G. Crystal structure refinement with SHELXL. *Acta Cryst. C*,2015, **71**, 3–8.

24 Farrugia, L.J. WinGX and ORTEP for windows: an update. *J. Appl. Cryst.*,2012, **45**, 8.

25 Spek, A.I. Single-crystal structure validation with the program PLATON. *J. Appl. Crystallogr.*,2003, **36**, 7–13.

26 M. Nardelli, *PARST*95-an update to *PARST*: a system of Fortran routines for calculating molecular structure parameters from the results of crystal structure analyses, *J. Appl. Cryst.*, 1995, **28**, 659.

27 Gavezzotti, A. Efficient computer modelling of organic materials. The atom–atom, Coulomb–London–Pauli (AA–CLP) model for intermolecular electrostatic–polarization, dispersion and repulsion energies. *New J. Chem.*,2011, **35**, 1360.

28 Gavezzoti, A. Calculation of intermolecular interaction energies by direct numerical integration over electron densities. 1. Electrostatic and polarization energies in molecular crystals. *J. Phys. Chem. B*,2002, **106**, 4145–4154.

29 Gavezzoti, A. Calculation of intermolecular interaction energies by direct numerical integration over electron densities. 2. An improved polarization model and the evaluation of dispersion and repulsion energies. *J. Phys. Chem. B*,2003, **107**, 2344–2353.

30 M. J. Frisch, G. W. Trucks, H. B. Schlegel, G. E. Scuseria, M. A. Robb, J. R. Cheeseman, G. Scalmani, V. Barone, G. A. Petersson, H. Nakatsuji, X. Li, M. Caricato, A. V. Marenich, J. Bloino, B. G. Janesko, R. Gomperts, B. Mennucci, H. P. Hratchian, J. V. Ortiz, A. F. Izmaylov, J. L. Sonnenberg, D. Williams-Young, F. Ding, F. Lipparini, F. Egidi, J. Goings, B. Peng, A. Petrone, T. Henderson, D. Ranasinghe, V. G. Zakrzewski, J. Gao, N. Rega, G. Zheng, W. Liang, M. Hada, M. Ehara, K. Toyota, R. Fukuda, J. Hasegawa, M. Ishida, T. Nakajima, Y. Honda, O. Kitao, H. Nakai, T. Vreven, K. Throssell, J. A. Montgomery, Jr., J. E. Peralta, F. Ogliaro, M. J. Bearpark, J. J. Heyd, E. N. Brothers, K. N. Kudin, V. N. Staroverov, T. A. Keith, R. Kobayashi, J. Normand, K. Raghavachari, A. P. Rendell, J. C. Burant, S. S. Iyengar, J. Tomasi, M. Cossi, J. M. Millam, M. Klene, C. Adamo, R. Cammi, J. W. Ochterski, R. L. Martin, K. Morokuma, O. Farkas, J. B. Foresman and D. J. Fox, *Gaussian 16, Revision C.01,* Gaussian, Inc., Wallingford, CT, 2016.

31 M. A. Spackman and J. J. McKinnon, Fingerprinting intermolecular interactions in molecular crystals, *CrystEngComm,* 2002, **4**, 378–392.

32 J. J. McKinnon, D. Jayatilaka and M. A. Spackman, Towards quantitative analysis of intermolecular interactions with Hirshfeld surfaces, *Chem. Commun.,* 2007, 3214–3816.

33 P. R. Spackman, M. J. Turner, J. J. McKinnon, S. K. Wolf, D. J. Grimwood, D. Jayatilaka and M. A. Spackman, Crystal Explorer: a program for Hirshfeld surface analysis, visualization and quantitative analysis of molecular crystal, *J. Appl. Cryst.,* 2021, **54**, 1006–1011.

34 J. J. McKinnon, M. A. Spackman and A. S. Mitchell, Novel tools for visualizing and exploring intermolecular interactions in molecular crystals. *Acta Crystallogr., Sect. B: Struct. Sci.*,2004, **60**, 627–668.

35 A. L. Rohl, M. Moret, W. Kaminsky, K. Claborn, J. J. Mckinnon and B. Kahr, Hirshfeld surfaces identify inadequacies in computations of intermolecular interactions in crystals: pentamorphic 1,8–dihydroxyanthraquinone, *Cryst. Growth Des.*,2008, **8**, 4517–4525.

36 P. Das, S. Islam and S. K. Seth, Structural elucidation and interpretation of 2D–3D supramolecular assemblies featuring lone-pair···π interaction in two Cu(II)–PDA complexes: experimental and computational assessment, *J. Mol. Struct.*, 2024, **1308**, 138088.

37 N. Abad, P. Das, J. T. Mague, A. Y. A. Alzahrani, E. M. Essassi. S. K. Seth and Y. Ramli, Exploring the solid-state structural aspects of novel hybrid quinoxaline based isoxazole compound: Inputs from experimental and computational studies, *J. Mol. Struct.*, 2025, **1324**, 140963.

38 S. P. Thomas, P. R. Spackman, D. Jayatilaka and M. A. Spackman, Accurate Lattice Energies for Molecular Crystals from Experimental Crystal Structures, *J. Chem. Theory Comput.*, 2018, **14**, 1614–1623.

39 R. F. W. Bader, A quantum theory of molecular structure and its applications, *Chem. Rev.,* 1991, **91**, 893–928.

40 T. A. Keith, *AIMAll (Version 13.05.06)*,TK Gristmill Software, Overland Park KS, USA, 2013.

41 R.F.W. Bader, *Atoms in Molecules: A Quantum Theory*, Oxford University Press, Oxford, UK, 1990.

42 C. Lepetit and M. L. Kahn, QTAIM and ELF topological analyses of zinc-amido complexes, *Res. Chem. Intermed.*, 2021, **47**, 377–395.

View Article Online
DOI: 10.1039/D5CE00838G

Data Availability Statement.

The data supporting this article have been included as part of the ESI. The crystallographic data for all the reported structures have been deposited in CSD and are available at https://www.ccdc.cam.ac.uk. The CCDC numbers are 2483272 – 2483275.